Theoretical basis for stabilizing messenger RNA through secondary structure design

Hannah K. Wayment-Steele[1,2], Do Soon Kim[2,3,5], Christian A. Choe[2,4], John J. Nicol[2], Roger Wellington-Oguri[2], R. Andres Parra Sperberg[4], Po-Ssu Huang[4], Eterna Participants[2], Rhiju Das[2,5,6]

[1] Department of Chemistry, Stanford University, Stanford, CA, 94305
[2] Eterna Massive Open Laboratory. Consortium authors listed in Table S1.
[3] Department of Chemical and Biological Engineering, Northwestern University, Evanston, IL, 60208
[4] Department of Bioengineering, Stanford University, Stanford, CA, 94305
[5] Department of Biochemistry, Stanford University, Stanford, CA, 94305
[6] Department of Physics, Stanford University, Stanford, CA, 94305

Abstract

RNA hydrolysis presents problems in manufacturing, long-term storage, world-wide delivery, and in vivo stability of messenger RNA (mRNA)-based vaccines and therapeutics. A largely unexplored strategy to reduce mRNA hydrolysis is to redesign RNAs to form double-stranded regions, which are protected from in-line cleavage and enzymatic degradation, while coding for the same proteins. The amount of stabilization that this strategy can deliver and the most effective algorithmic approach to achieve stabilization remain poorly understood. Motivated by the need for stabilized COVID-19 mRNA vaccines, we present simple calculations for estimating RNA stability against hydrolysis, and a model that links the average unpaired probability of an mRNA, or AUP, to its overall rate of hydrolysis. To characterize the stabilization achievable through structure design, we compare optimization of AUP by conventional mRNA design methods to results from the LinearDesign algorithm, a new Monte Carlo tree search algorithm called RiboTree, and crowdsourcing through the OpenVaccine challenge on the Eterna platform. Tests were carried out on mRNAs encoding nanoluciferase, green fluorescent protein, and COVID-19 mRNA vaccine candidates encoding SARS-CoV-2 epitopes, spike receptor binding domain, and full-length spike protein. We find that Eterna and RiboTree significantly lower AUP while maintaining a large diversity of sequence and structure features that correlate with translation, biophysical size, and

immunogenicity. Our results suggest that increases in in vitro mRNA half-life by at least two-fold are immediately achievable and that further stability improvements may be enabled with thorough experimental characterization of RNA hydrolysis.

Introduction

Messenger RNA (mRNA) molecules have shown promise as vaccine candidates in the current COVID-19 pandemic (1-3) and may enable a large number of new therapeutic applications (4-6). However, a major limitation of mRNA technologies is the inherent chemical instability of RNA. mRNA manufacturing yields are reduced by degradation during in vitro transcription; mRNA vaccines stored in solution require in vitro stability, ideally over months under refrigeration (7); RNA vaccines deployed in developing regions would benefit from increased in vitro stability against high temperatures (8); and after being administered, mRNA vaccines require stabilization against hydrolysis and enzymatic degradation to sustain translation and immunogenicity in the human body (9).

RNA degradation depends on how prone the molecule is to in-line hydrolytic cleavage and attack by nucleases, oxidizers, and chemical modifiers in the RNA's environment (10-13). Amongst these degradation processes, in-line hydrolytic cleavage is a universal mechanism intrinsic to RNA. Cleavage of an RNA backbone phosphodiester bond is initiated by deprotonation of the 2'-hydroxyl group of the ribose moiety (14) (Figure 1A). The deprotonated hydroxyl group attacks the phosphate to form a pentacoordinate transition state. The formation of this transition state relies on the RNA backbone being able to adopt a conformation where the 2'- hydroxyl group is in line with the leaving 5' oxyanion. The 5' oxyanion then departs and generates a 2',3'-cyclic phosphate. The same mechanism underlies

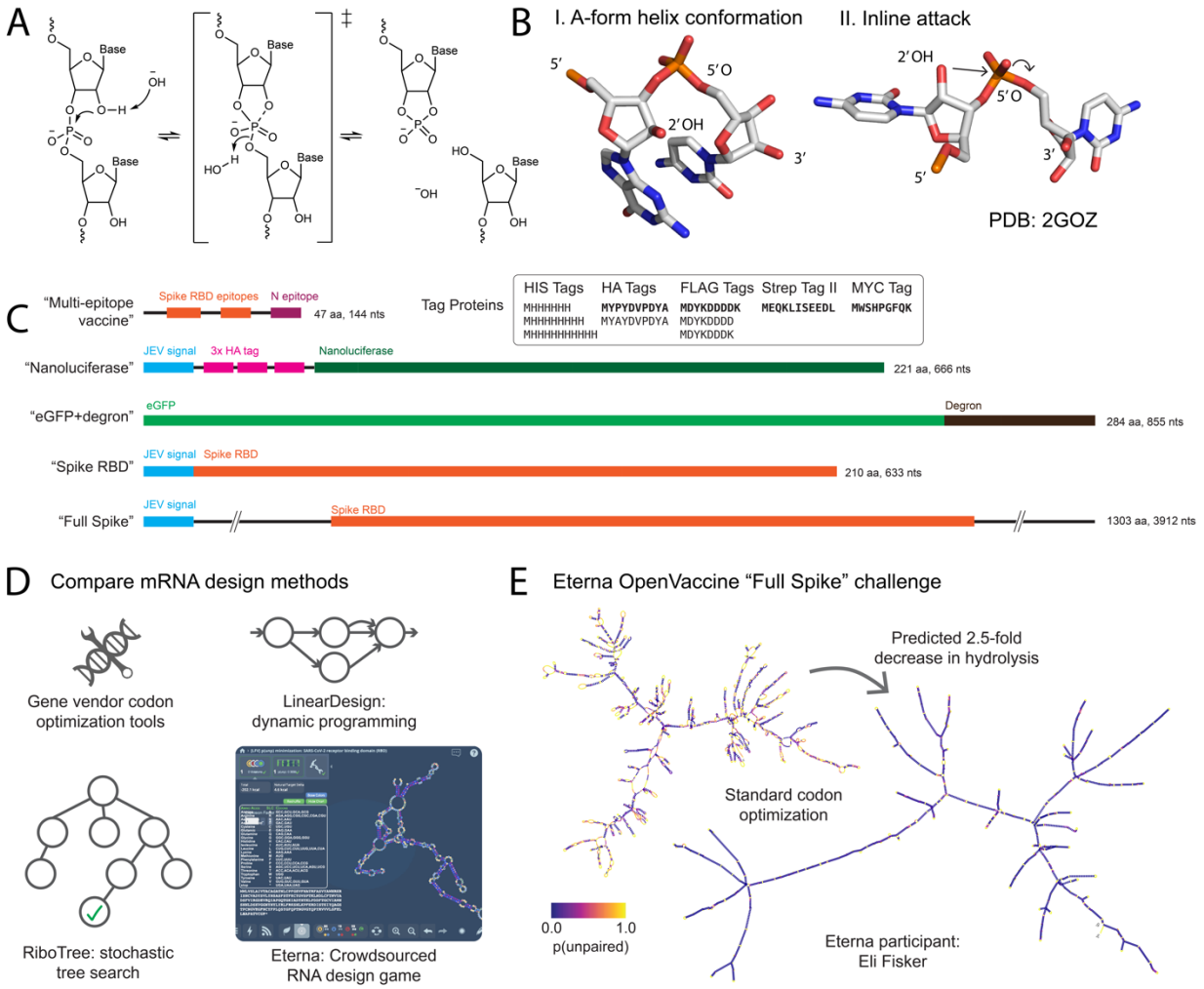

Figure 1. (A) Hydrolysis of the phosphodiester bond in the RNA backbone bond. This mechanism proceeds via an "inline attack" backbone conformation, depicted in (B): the attacking 2'-hydroxyl group is in line with the phosphate group and the leaving 5' oxygen. (C) Sequence schematics of all mRNA design challenges in this work. (D) We compared the maximum degree of stabilization achievable through a variety of current and novel design methods. (E) mRNAs designed by conventional means for therapeutics are prone to hydrolysis in regions that have low probability of being unpaired (shown in yellow, left panel). A design for a vaccine design based on the mRNA of the SARS-CoV-2 full spike protein (right panel) with the optimal found value for the metric presented in this work, the average unpaired probability (AUP).

the action of self-cleaving ribozymes and protein-based nucleases, allowing this conformation to be characterized experimentally and visualized in crystal structures (Figure 1B, structure from ref. (15)).

The World Health Organization's target product profile for vaccines calls for formulations that remain effective after a month under refrigeration (8). Deployment of mRNA vaccines for infectious disease outbreaks like the current COVID-19 pandemic would benefit from taking advantage of existing

supply networks for conventional attenuated vector vaccines, which are set up for pre-filled syringes in saline buffer at near-neutral pH under refrigeration (8). Does RNA hydrolysis impact the viability of RNA molecules in the above context? To address these questions, we present calculations based on the model of Li & Breaker (16) for RNA phosphodiester bond cleavage as a function of pH, temperature, and ionic concentration, summarized in Table 1.

Under refrigerated transport conditions ('cold-chain', 5 °C, phosphate-buffered saline, pH 7.4, no Mg^{2+}) (8), a naked RNA molecule encoding a SARS-CoV-2 spike glycoprotein, with a length of roughly 4000 nucleotides in bulk solution would have a half-life of 900 days, with 98% intact after 30 days. We note therefore that, "naked" mRNA molecules are in fact expected to be stable after a month under refrigeration, fitting the target product profile for vaccines from the World Health Organization. However, difficulties may arise in practice. A temperature excursion to 37 °C is predicted to lead to a half-life reduced to 5 days, well under a month. Even if temperature can be maintained at 5˚C, RNAs encapsulated in lipid formulations may be subject to increased hydrolysis if the lipid's cationic headgroups lower the pKa of the ribose 2-hydroxyl group (17, 18). If pKa shifts as small as 2 units occur, the predicted half-life reduces from 900 days to 10 days, again well under a month (Table 1).

Beyond these calculations under storage and shipping conditions, an mRNA vaccine will be unstable to hydrolysis at other stages of its use. During its production, the mRNA is subjected to conditions optimized for high synthesis. Under conditions typically used for in vitro transcription by T7 bacteriophage RNA polymerase, the presence of Mg^{2+} (at 10-20 mM) and temperature of 37 °C leads to a half-life estimate of 2 hours for a 4000-nt mRNA (Table 1). Even if hydrolysis is mitigated by lower Mg^{2+}, pH, and temperature, significant degradation is therefore expected to occur during transcriptions of 1-2 hours (19), substantially lowering yields after purification. Finally, the mRNA is susceptible to hydrolysis upon delivery into the human body. There, the presence of Mg^{2+} ions, estimated to have a

free concentration of 1 mM (20), a temperature of 37 °C, and pH of 7.4 are predicted to give a half-life of 5 days, providing a biochemical limit to how long the mRNA will last as an agent for translation in vivo.

Beyond the above calculations for a ~4000 nt mRNA, the longer lengths of RNA molecules being considered for low-material-cost 'self-amplifying' mRNA (SAM) vaccines (3, 21) are expected to exacerbate inline hydrolysis. In all conditions described above, the half-life will be reduced by 3-fold compared to a non-SAM mRNA. As an example, if during storage or shipment at pH 7.4, the SAM vaccine of length 12 kB is subject to an excursion of temperature to 37 °C for 2 days, the fraction of functional, full-length mRNA remaining after that excursion will drop to less than half of the starting RNA (Table 1).

Simulated condition (0.14 M [K^+])	**T (°C)**	**pH**	**[Mg^{2+}] (mM)**	**RNA length (nucleotides)**	**AUP[a]**	**Cleavage rate per molecule (k_{deg}) (10^{-7} min^{-1})**	**Half-life[b] (days)**
Refrigerated supply chain ('cold chain')	5	7.4	0	4,000	0.4	5.1	941
Refrigerated supply chain, increased length (SAM RNA)	5	7.4	0	12,000	0.4	15.3	314
Refrigerated supply chain, pKa shifted by cationic formulation	5	9.4[c]	0	4,000	0.4	470	10.2
Temperature excursion	37	7.4	0	4,000	0.4	890	5.4
Manufacturing (in vitro transcription)[d]	37	7.6	14	4,000	0.4	57,000	0.084
Physiological	37	7.4	1[e]	4,000	0.4	2,000	2.4

[a] Standard AUP of 0.4 estimated from standard design methods studied in this work.
[b] Calculated as $t_{1/2} = \ln 2 / k_{deg}$.
[c] Apparent pH at 2′ hydroxyl, assuming pK_a shift of 2 units induced by complexation with cationic lipid.
[d] Ref. (19), with pH 7.9 of Tris-HCl buffer corrected from 25 °C to 37 °C.
[e] Ref. (20).

Table 1. Estimates for RNA degradation using the quantitative model presented by Li & Breaker (14) and the model for AUP presented in this work.

The calculations above assume that the RNA sequence and structure are not specially designed to resist degradation. One largely unexplored design method to reduce RNA hydrolysis that is independent of mRNA manufacturing, formulation, storage, and *in vivo* conditions is to increase the degree of

secondary structure present in the RNA molecule. Hydrolysis has been found to be mitigated by the presence of secondary structure, which restricts the possible conformations the backbone can take and reduces the propensity to form conformations prone to in-line attack (22). Indeed, the technique of inline probing takes advantage of the suppression of in-line hydrolysis within double-stranded or otherwise structured regions to map RNA structure (23).

As part of the OpenVaccine project based at Stanford University and the Eterna platform, we are seeking rapid improvements to mRNA stability and function that might have an impact on the current COVID-19 pandemic. Here, we report a theoretical framework and computational results that have motivated ongoing experimental studies in COVID-19 mRNA vaccine stabilization. We present a simple model that links an RNA molecule's overall hydrolysis rate to base-pairing probabilities, which are readily calculated in widely used modeling packages (24-27). We define two metrics: the Summed Unpaired Probability of a molecule, or SUP, and the Average Unpaired Probability, or AUP, which is the SUP normalized by sequence length. By comparing a variety of mRNA design methods (Figure 1D), we provide evidence that both crowdsourced rational design on the Eterna platform and a new stochastic optimization algorithm, RiboTree, are able to minimize AUP for the CDS of larger mRNAs that have too many synonymous sequences to allow for enumeration. The calculations predict that such structure-optimizing designs can achieve at least two-fold increases in estimated mRNA half-life (Figure 1E), independent of the mRNA length. Our results furthermore suggest that optimizing for mRNA half-life can be carried out while retaining other desirable sequence or structure properties of the mRNA, such as codon optimality, short stem lengths, and compactness measures, which may modulate in vivo mRNA translation and immune response. We conclude by discussing immediate implications for stabilizing RNA therapeutics, further extensions of our analysis, and further experiments that would advance computational design of stabilized messenger RNA.

Results

A biophysical model for RNA degradation. Previous studies have explored the design of mRNA molecules with increased secondary structure (28-30), as evaluated by the predicted folding free energy of the mRNA's most stable structure, but it is unclear if this metric is the correct one when improving stability of an RNA against degradation. Our computational studies are based on a simple, principled model of RNA degradation that suggests an alternative metric. To describe the degradation rate of an RNA molecule, we imagine that each nucleotide at position *i* has a rate of degradation $k_{cleavage}(i)$ that we approximate as staying constant over time. To focus our presentation, we imagine that the degradation is due to inline hydrolysis, but the framework below generalizes to any degradation process that is suppressed by formation of RNA structure. The probability that the nucleotide backbone remains intact at nucleotide *i* after time *t* is

$$p_{intact}(i,t) = e^{-k_{cleavage}(i)\,t}. \qquad (1)$$

The probability that the overall RNA with length *N* remains intact with no chain breaks after time *t* is then

$$p_{intact}{}^{overall}(t) = \prod_{i=1}^{N} p_{intact}(i,t) = \prod_{i=1}^{N} e^{-k_{cleavage}(i)t}$$
$$= \exp(-\sum_{i=1}^{N} k_{cleavage}(i)\,t). \qquad (2)$$

Here, we have assumed that the probability of cleavage at any given position is independent of cleavage events at other positions in the RNA. If this is not true, the expression will still remain correct at times when there are 0 or 1 cleavage events, and that is the time range most relevant for improving RNA

stability. Given that assumption, eq. (2) gives an exactly exponential dependence of the overall degradation of the RNA with respect to time *t*:

$$\mathrm{p}_{\mathrm{intact}}^{overall}(t) = e^{-k_{cleavage}{}^{overall}t}, \tag{3}$$

with

$$k_{cleavage}{}^{overall} = \sum_{i=1}^{N} k_{cleavage}(i). \tag{4}$$

The rate at which an RNA is hydrolyzed at a specific location along its backbone depends on the ability of the phosphodiester bond to adopt the in-line attack conformation (Figure 1B), or more generally for the RNA to adopt a conformation that can be accessed by a degrading agent, like a protein nuclease. Here and below, we work out the consequences of a simple model reflecting the knowledge that in-line hydrolysis generally occurs at nucleotides that are unpaired but is strongly suppressed by pairing of the nucleotide into double-stranded segments of the secondary structure. Since RNA chains fluctuate between multiple secondary structures, we write the overall cleavage rate as averaged over the structural ensemble of the RNA,

$$k_{cleavage}{}^{overall} = \sum_{s\in\{S\}} p(s) \sum_{i} k_{cleavage}(i|s), \tag{5}$$

where {*S*} is the full set of structures that the RNA molecule is capable of adopting, and $p(s)$ is the probability of forming a structure *s*. The rate of cleavage $k_{cleavage}(i|s)$ at each position *i* within a structure *s* will, in general have a complex dependence on the sequence and structural context, e.g., whether the nucleotide is in a hairpin loop, where it is in within the loop, whether other loop nucleotides might promote in-line cleavage through acid-base catalysis, whether the loop has non-canonical pairs, etc. Without additional empirical knowledge, we assume that the cleavage rate for

unpaired nucleotides can be approximated by a constant rate $k_{cleavage}^{unpaired}$ if nucleotide *i* is unpaired, and zero if paired. Then eq. (5) becomes:

$$\begin{aligned} k_{cleavage}^{overall} &= \sum_{s\in\{S\}}\sum_i \; p(s)\, k_{cleavage}(i|s) \\ &= \sum_i \sum_{s\in\{S\}} p(s) k_{cleavage}(i|s) \\ &= \sum_i \; \sum_{s\in\{S\}} p(s) I(i \text{ unpaired in } s)\, k_{cleavage}^{unpaired} \\ &= k_{cleavage}^{unpaired} \sum_i \; p_{unpaired}(i) \\ &= k_{cleavage}^{unpaired} \times \text{SUP}, \end{aligned} \qquad (6)$$

where $I(i \text{ unpaired in } s)$ is 1 if nucleotide *i* is unpaired in the structure *s* and 0 otherwise. In the last line of (6), we introduce the definition of Sum of Unpaired Probabilities,

$$\text{SUP} = \sum_i \; p_{unpaired}(i). \qquad (7)$$

Overall, the total rate of cleavage may be approximated as this measure, the sum of unpaired probabilities across all nucleotides of the RNA, multiplied by a constant that reflects the average cleavage rate of an unpaired nucleotide.

It is important to point out that the total rate scales with the sum of the unpaired probabilities of the RNA's nucleotides – longer RNA molecules are expected to degrade faster in proportion to their length. This relation is better reflected by a rearrangement of (6) to:

$$k_{cleavage}^{overall} = k_{cleavage}^{unpaired} \times N \times \text{AUP} \qquad (8)$$

where the average unpaired probability (AUP) is

$$\text{AUP} = \frac{1}{N}\sum_i \; p_{unpaired}(i) = \frac{1}{N}\,\text{SUP}. \qquad (9)$$

The AUP value is a number between 0 and 1 that reflects the overall 'structuredness' of the RNA. Lower values correspond to lower probability of being unpaired, and therefore RNA molecules less susceptible to degradation.

In these last expressions (eqns. 6-9), $p_{unpaired}(i)$ can be predicted in most widely-used RNA secondary structure prediction packages, which output base pair probabilities $p(i:j)$, the probability that bases *i* and *j* are paired. Then the probability that any nucleotide *i* is unpaired in the RNA is given as

$$\text{SUP} = \sum_{i=1}^{N}\left[1 - \sum_{j=1}^{N} p(i:j)\right],$$

$$\text{AUP} = \text{SUP} / N. \qquad (9)$$

Under this model, it becomes possible to computationally explore the question of how much an RNA might be stabilized if it is redesigned to form stable secondary structures, which we describe next.

Small mRNA models reveal discrepancy in sequences optimized for SUP vs. sequences optimized for codon optimality or minimum folding free energy.

To investigate the possible practical significance and dynamic range of the SUP/AUP metrics presented above, we started with mRNA design problems that were small enough to be tractable, i.e., all mRNA sequences that code for the target amino acid sequence could be directly enumerated and studied. We selected a collection of short peptide tags that are commonly appended or prepended to proteins to enable purification or imaging: His tags of varying lengths, human influenza hemagglutinin (HA) tag,

Strep-tag II, FLAG fusion tag, and Myc tag sequences (31), and enumerated all the mRNA sequences that encode each protein. For reference, we also generated sequences from online codon optimization tools from IDT, GENEWIZ, and Twist (see Methods). We calculated a variety of sequence-based and thermodynamic metrics for each sequence. Here and below, we note that AUP and SUP are proportional within sets of solutions for a given mRNA design problem, and we typically present AUP. We also note that our results focus on redesigning the CDS regions only of the mRNA; extension to (the typically smaller) 5′ and 3′ untranslated regions is discussed below.

We first compared the AUP of solutions from vendor sequences to the AUP of all enumerated sequences (Figure 2A, Figure S1). Notably, solutions that maximize codon adaptation index (CAI), a commonly used metric for codon usage that has been proposed to correlate with protein translation rates (32, 33) and underlies several vendor algorithms, do not reliably result in minimal AUP values. Structures of mRNA sequences from the vendor GENEWIZ, which all achieve a maximal CAI of 1.0, are shown in Figure 2B, and exhibit unpaired loops.

We next used these enumerated sequences to compare the minimal AUP solution to the solution whose minimum free energy structure (MFE) had the lowest folding free energy relative to a fully unfolded state, ΔG(MFE), a metric that is commonly used as a proxy for 'structuredness' (28-30). For 4 of the 10 model systems studied – the three His tags and the FLAG tag – the coding sequence with the lowest free energy MFE structure also exhibited the lowest AUP (Figure 2A, Figure S1).

However, for other model proteins, including the Strep-tag II, the HA tag, and the Myc tag, the coding sequence with the lowest-energy MFE structure was not the same as the solution with the lowest AUP (Figure 2A). The most notable difference was in designs for the HA tag: the lowest AUP value

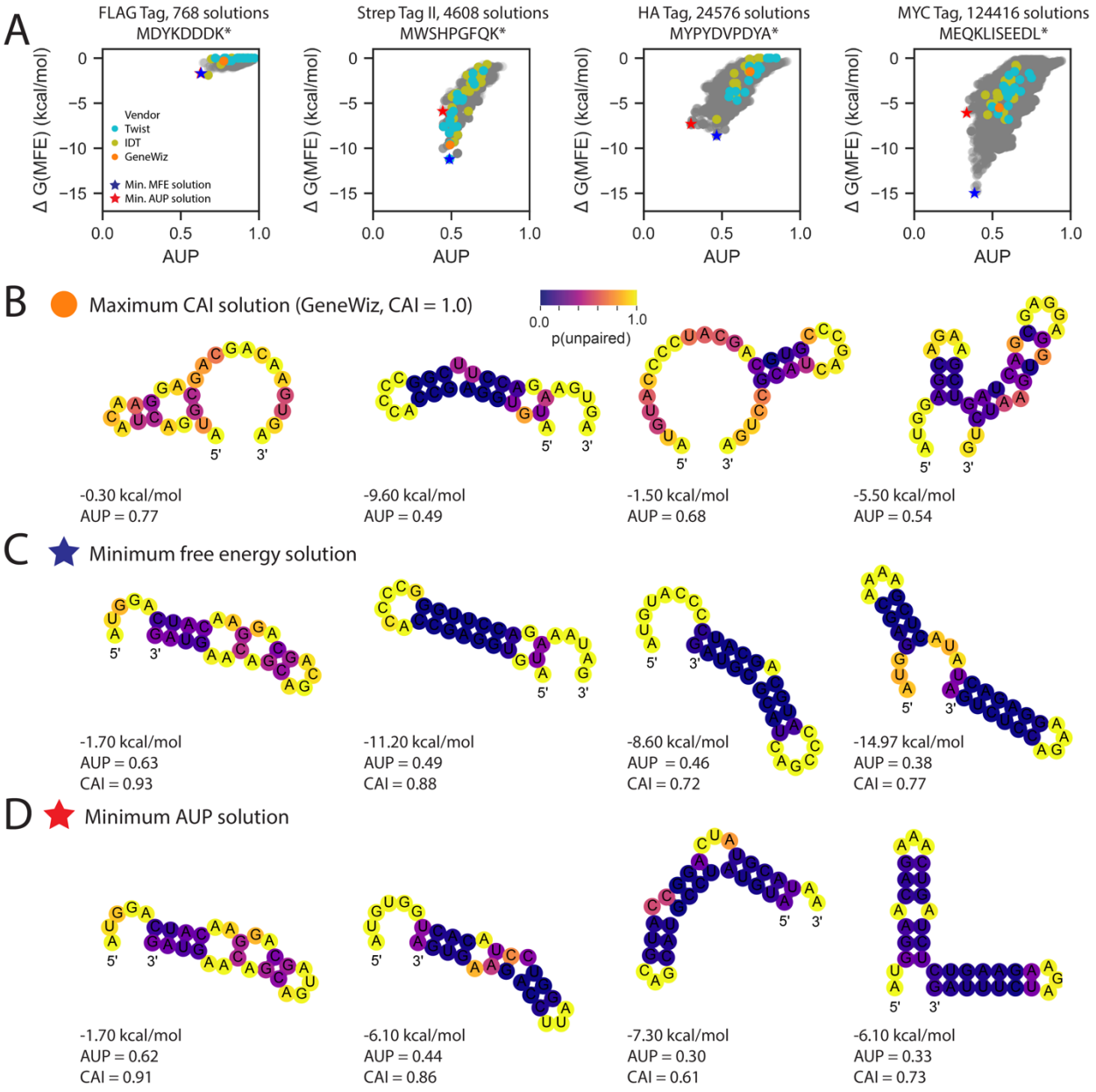

Figure 2. (A) Enumerating all possible coding sequences for small tag proteins reveals that the coding sequence with the lowest energy for its MFE structure (blue star) is not always the same as the coding sequence with the lowest AUP (red star). In (B) – (D), MFE structures for mRNA solutions are shown, with nucleotides are colored by p(unpaired). (B) Sequences from vendors optimizing for codon usage do not reliably minimize ΔG(MFE) or AUP. The mRNA with the lowest-energy MFE structure is displayed in (C), and the mRNA with the lowest AUP is displayed in (D).

obtained was 0.30, which is 1.5-fold lower than AUP of the minimal MFE solution, 0.46. Comparing the MFE structures of the two solutions reveals changes in structure that result in a higher free energy but a lower AUP (Figure 2C, 2D). Intuitively, if we wish to reduce overall hydrolysis, it is better for the RNA to

have more stems and fewer 'hot spots' (5 vs. 15 yellow nucleotides in HA panel of Figures 2D vs. 2C) than to optimize the folding free energy of each stem, once formed (reflected here in the base pairing probability; magenta vs. dark purple coloring in HA panel of Figures 2D vs. 2C). Furthermore, the min. AUP solutions have CAI values of 0.91, 0.86, 0.61, and 0.73 respectively, which are comparable to vendor-generated sequences, suggesting that optimization of AUP will not result in a major penalty on CAI. Repeating the same analysis across other small model systems as well as with other secondary-structure packages (27, 34) reveals similar results (Figure S1).

How much can these small mRNAs be stabilized over standard mRNA design methods? We calculated the change in AUP obtained between the average of all the vendor-returned sequences and the minimum AUP solution for tag proteins, and found fold-changes in AUP ranging from 1.27 to 2.23-fold decrease in AUP (Table 2). This enumerative analysis of small model mRNAs suggested up to 2-fold increased stabilization might be achievable in mRNA design while retaining codon optimality, at least for small sequences.

	FLAG Tag	**Strep Tag II**	**HA Tag**	**MYC Tag**
Protein length	8	9	10	11
mRNA CDS length[a]	27	30	33	36
# Synonymous mRNAs	768	4,608	24,576	124,416
Standard methods[b], mean(std). AUP	0.86(7)	0.57(7)	0.67(9)	0.60(6)
Standard methods[b], min. AUP	0.68	0.45	0.47	0.45
Global Min. AUP	0.62	0.44	0.30	0.33
Mean standard / Global Min.	1.39	1.30	2.23	1.82
Min standard / Global Min.	1.10	1.02	1.57	1.36

[a] mRNA length = 3 × protein length + 3 (stop codon).
[b] GENEWIZ, IDT, Twist.

Table 2. AUP values for example tag proteins and calculated fold-change decrease in AUP from standard design methods to the global min. AUP value.

A two-fold decrease in AUP is achievable for long mRNA constructs.

To accommodate a broad application of our hypothesis for mRNAs, we tested a variety of target proteins with lengths of hundreds of nucleotides, some with therapeutic potential against SARS-CoV-2 and some commonly used in laboratory settings and animal studies to test protein synthesis levels

(Figure 1C). The four systems were a multi-epitope vaccine design (MEV) derived from SARS-CoV-2 spike (S) and nucleocapsid (N) proteins; Nanoluciferase; enhanced green fluorescence protein with an attached degron sequence (eGFP+deg), used by Mauger et al. for characterizing mRNA stability and translation; and the receptor binding domain (RBD) of the SARS-CoV-2 spike protein. We compared sequences generated by a variety of methods (Figure 1D): uniform sampling of codons ("Uniform random codons"); uniform sampling of GC-rich codons only ("GC-rich codons"); vendor-supplied servers from IDT, GENEWIZ, and Twist; and the algorithm LinearDesign (29), which returns a sequence with minimal ΔG(MFE) solution that is balanced with codon usage, as well as sequences from other groups when possible (35). We further developed a stochastic Monte Carlo Tree Search algorithm, RiboTree, to stochastically minimize AUP of model mRNAs. Finally, we crowdsourced solutions through the online RNA design platform Eterna (36).

Eterna is currently carrying out the OpenVaccine challenge, a series of projects to optimize COVID-19 mRNA vaccines with high-throughput experimental feedback. We were optimistic that Eterna participants could achieve low AUP values after observing low AUP values for constructs collected from early Eterna vaccine design challenges. These earlier challenges, labeled "Eterna, exploratory" in Figures 3 and 4, were not set up with any specific optimization targets other than a general call to create mRNAs that coded for the target proteins but formed significant structures in Eterna's game interface, which provides folding calculations in a number of secondary structure prediction packages. An additional set of Eterna sequences were solicited in the "p(unp) challenges", where the AUP metric was calculated and provided to Eterna participants within the game interface to guide optimization. The protein targets of the mRNA design challenges described in Methods, and sequences are listed in Table S2. As in the previous section, we did not explore design of the 5' or 3' untranslated regions or design principles intended to minimize structure at the start site of the CDS.

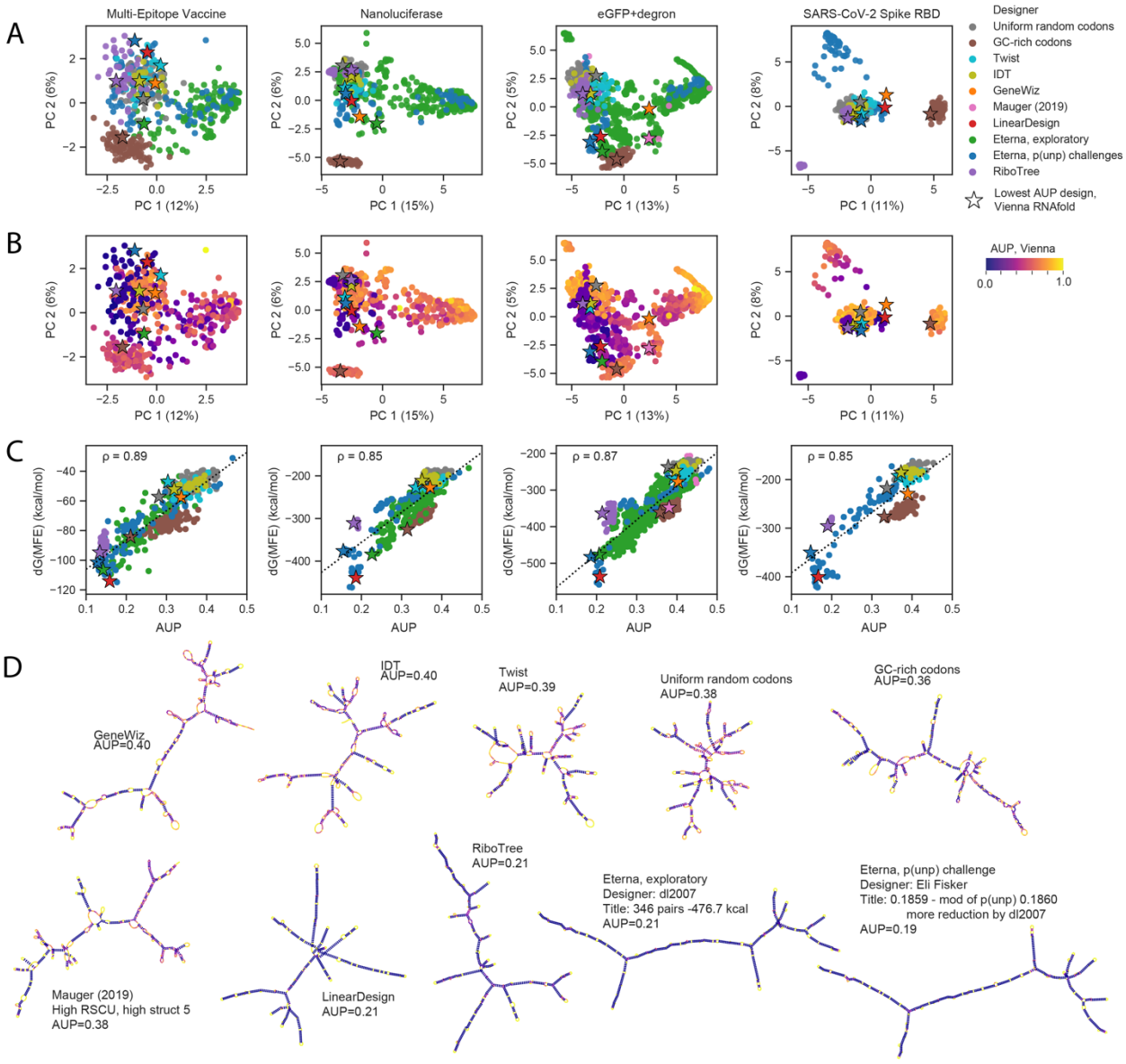

Figure 3. Sequences designed rationally by participants during Eterna's OpenVaccine challenge result in the lowest AUP values for mRNAs encoding a variety of model proteins used for studying translation and as model vaccines, ranging in length from 144 nucleotides (the Multi-epitope Vaccine) to 855 nucleotides (eGFP+degron (35)). (A) Eterna designs encompass a diverse sequence space when compared to mRNA sequences generated by random sampling, visualized with a principal component analysis. (B) The same visualization, colored by AUP as calculated in ViennaRNA. (C) While ΔG(MFE) and AUP are correlated, the design with the lowest AUP is not the same as the design with the lowest ΔG(MFE). Starred points indicate the design for each design strategy with the lowest AUP value, calculated with ViennaRNA. (D) Force-directed graph visualization of sequences coding for eGFP+degron with lowest AUP value from each design source, colored by AUP per nucleotide.

mRNA design challenge	Multi-epitope vaccine	Nanoluciferase	eGFP + degron	Spike RBD	Full Spike
Protein length (aa)	47	221	284	210	1303
mRNA CDS length (nt)	144	666	855	633	3912
Standard methods[b], mean(std) AUP	0.34(4)	0.36(2)	0.40(2)	0.39(2)	0.40(2)
Standard methods[b], min. AUP	0.21	0.31	0.36	0.33	0.36
Stabilizing methods[c], mean(std) AUP	0.19(7)	0.22(7)	0.26(7)	0.22(7)	0.20(5)
Stabilizing methods[c], min. AUP[d]	0.13	0.15	0.19	0.15	0.17
Mean standard / mean stabilizing	1.78	1.64	1.56	1.74	1.95
Min. standard / min. stabilizing	1.64	2.03	1.92	2.24	2.16
Mean standard / min stabilized	2.65	2.36	2.17	2.65	2.40

[a] mRNA length = 3 × protein length + 3 (stop codon).
[b] Uniform codons, GC codons, GENEWIZ, IDT, Twist.
[c] Eterna p(unp) challenge, RiboTree, LinearDesign.
[d] In all cases, minimal AUP was achieved in Eterna p(unp) challenge.

Table 3. Statistics of AUP values obtained in comparing different classes of design methods on mRNA design challenges in this study.

We found that designs from the tested algorithmic and crowdsourcing approaches encompassed a range of sequence space, comparable to the sequence diversity observed in the random sampling control sets (Figure 3A), as visualized through principal component analysis (PCA). Furthermore, sequences with low AUP values did not localize to specific regions of sequence space (Figure 3B). This diversity at the sequence level was also reflected in diversity in structures, as is further discussed below.

For all four challenges, the sequences with the lowest AUP values were designed by Eterna participants (Figure 3C). Figure 3D depicts MFE structures of the minimal AUP sequence for each design method for the eGFP+degron challenge (the longest mRNA), with nucleotides colored by their unpaired probability, as calculated in the ViennaRNA folding package. MFE structures of minimal AUP sequences

from each mRNA challenge are in Figure S2. Structures portrayed in Figure 3D indicate visual hallmarks of structures with lower AUP: solutions from LinearDesign, RiboTree, and Eterna have longer helices, fewer loops and junctions, and lower unpaired probabilities in stems (indicated by darker blue). Table 3 contains summary statistics for AUP values for design methods separated by standard methods (codon sampling, gene vendor tools) and methods intended to stabilize secondary structure (Eterna p(unp) rational design, LinearDesign, RiboTree).

The distributions of all Eterna participant submissions in the "p(unp) challenge" (mean and standard deviations of MEV: 0.22 ± 0.08, Nluc: 0.24 ± 0.08, eGFP: 0.28 ± 0.08, Spike RBD: 0.24 ± 0.08) were significantly lower than values from standard methods, including codon random sampling and vendor-generated sequences (MEV: 0.34 ± 0.04, Nluc: 0.36 ± 0.02, eGFP: 0.40 ± 0.02, Spike RBD: 0.39 ± 0.02, Table 3). The lowest AUP values from Eterna participants (MEV: 0.128, Nluc: 0.155, eGFP: 0.186, Spike RBD: 0.148) were lower in each case than the AUP values of LinearDesign constructs, (MEV: 0.159, Nluc: 0.186, eGFP: 0.208, Spike RBD: 0.167), or of minimum AUP solutions from RiboTree (MEV: 0.134, Nluc: 0.181, eGFP: 0.214, Spike RBD: 0.190). RiboTree came closest (within 5%) to the minimal Eterna AUP value for the shortest mRNA sequence, suggesting that RiboTree was better able to search sequence space for the shorter sequences. One of the challenges, the eGFP+degron mRNA, could be compared to designs developed by Mauger et al. based on folding free energy optimization to increase functional lifetime in human cells (35). The minimal AUP value from those sequences was 0.381, was similar to the value obtained from randomly-sampled codons, suggesting that explicit optimization of AUP is necessary for applications seeking stability against hydrolysis. Repeating these analyses of mRNAs with other secondary-structure packages reveals similar results (Figure S3).

We were interested to note that RiboTree solutions exhibited low AUP while not necessarily minimizing ΔG(MFE). Minimum AUP solutions from RiboTree had absolute ΔG(MFE) values that were up to 75% reduced from the absolute ΔG(MFE) values of minimum AUP solutions from Eterna participants

(MEV: 93%, Nanoluciferase: 82%, eGFP+deg: 75%, Spike RBD: 84%). Minimizing AUP without minimizing ΔG(MFE) may prove to be a valuable design strategy for developing mRNAs that are stable under storage but need to be unstable once inside human cells to enable unfolding by the cells' translational apparatus.

Diversity of properties related to translation and immunogenic function. After establishing the feasibility of designing mRNA sequences with reduced AUP, we wished to determine if these sequences might be viable for translation and for either preventing or eliciting innate immune responses. In advance of experimental tests, we tabulated sequence and structure properties that have been hypothesized to correlate with translation and immunogenicity.

We first characterized the codon adaptation index (CAI) of sequences across design methods, as this measure has been implicated in improving translation efficiency. We found that across all p(unp) challenges, minimal AUP sequences consistently had CAI values greater than 0.7 (Figure 4A), suggesting that it is feasible to design low AUP sequences that are translatable, at least as assessed by a widely used metric. Another important consideration is the possibility of mRNA therapeutics eliciting immunogenic responses from pathways that recognize double-stranded RNA helices. We found that none of the sequences characterized included helices longer than 33 base pairs, a measure that has been found to be the minimum length that leads to global shutdown of cellular mRNA translation after sensing by protein kinase R (37) (Figure 4B). Importantly, however, different designs exhibited a wide spectrum of helix lengths (8 to 22 base pairs, Figure 4B), suggesting that a less drastic innate immune response might be achieved, and be tunable depending on whether such responses are desirable (mRNA vaccines) or not (e.g., for anti-immune mRNA therapeutics).

In addition to the stability against hydrolysis, translatability and immunogenicity of mRNA therapeutic molecules, we expect there are many structural characteristics that relate to a molecule's in

vivo persistence that are not yet well understood. The ability to design multiple low-AUP sequences with a large range of alternative structures increases the potential that a functional design may be found in empirical tests or as the connections between mRNA structure and function are better understood. For instance, in Figure 3D, we observed that although LinearDesign, RiboTree, and Eterna sequences for an eGFP+degron mRNA all have AUP values within 10% of each other, they have different secondary structures. The same can be seen for all the mRNA design problems we probed (Figure S2).

As a quantitative evaluation of structural diversity, we characterized the Maximum Ladder Distance (MLD) of designed sequences. This measure has been used to describe the compactness of viral genomic RNAs and has been hypothesized to be relevant for viral packaging, immunogenicity, and biological persistence (37-40). If an RNA molecule's secondary structure is represented as an undirected graph, where edges represent helices, with edge lengths corresponding to helix lengths, and vertices correspond to loops, the MLD is the longest path that can be traced in the graph. Genomic viral RNAs have been demonstrated to have shorter MLDs than equivalent random controls, and molecules with shorter MLDs have been shown to be more compact experimentally, a feature that may also contribute to persistence (39).

We found that AUP and MLD were negatively correlated across the MEV, Nanoluciferase, eGFP+degron, and Spike RBD challenges (-0.64, -0.59, -0.62, -0.70, respectively, Figure 4C). This overall (negative) correlation reflects how minimizing AUP leads to larger average MLD values – but we note that the MLD values still fall over a wide range for sequences with low AUP. Example structures from the Nanoluciferase challenge are depicted in Figure 4D, the challenge that showed the widest range of MLD values for low AUP structures, which range from highly branched, compact structures (Figure 4D, left) to long, snake-like structures (Figure 4D, right). These structures exhibit uniformly low unpaired probabilities in stems (indicated by dark blue coloring), with the main difference being the layout of stems. These sequences demonstrate that both automated and rational design methods are capable of

finding RNA sequences with both low AUP values and a range of MLD values. Testing these mRNAs experimentally for their translation rates and persistence in cells and in animals will help address the relationship between MLD and mRNA therapeutic stability.

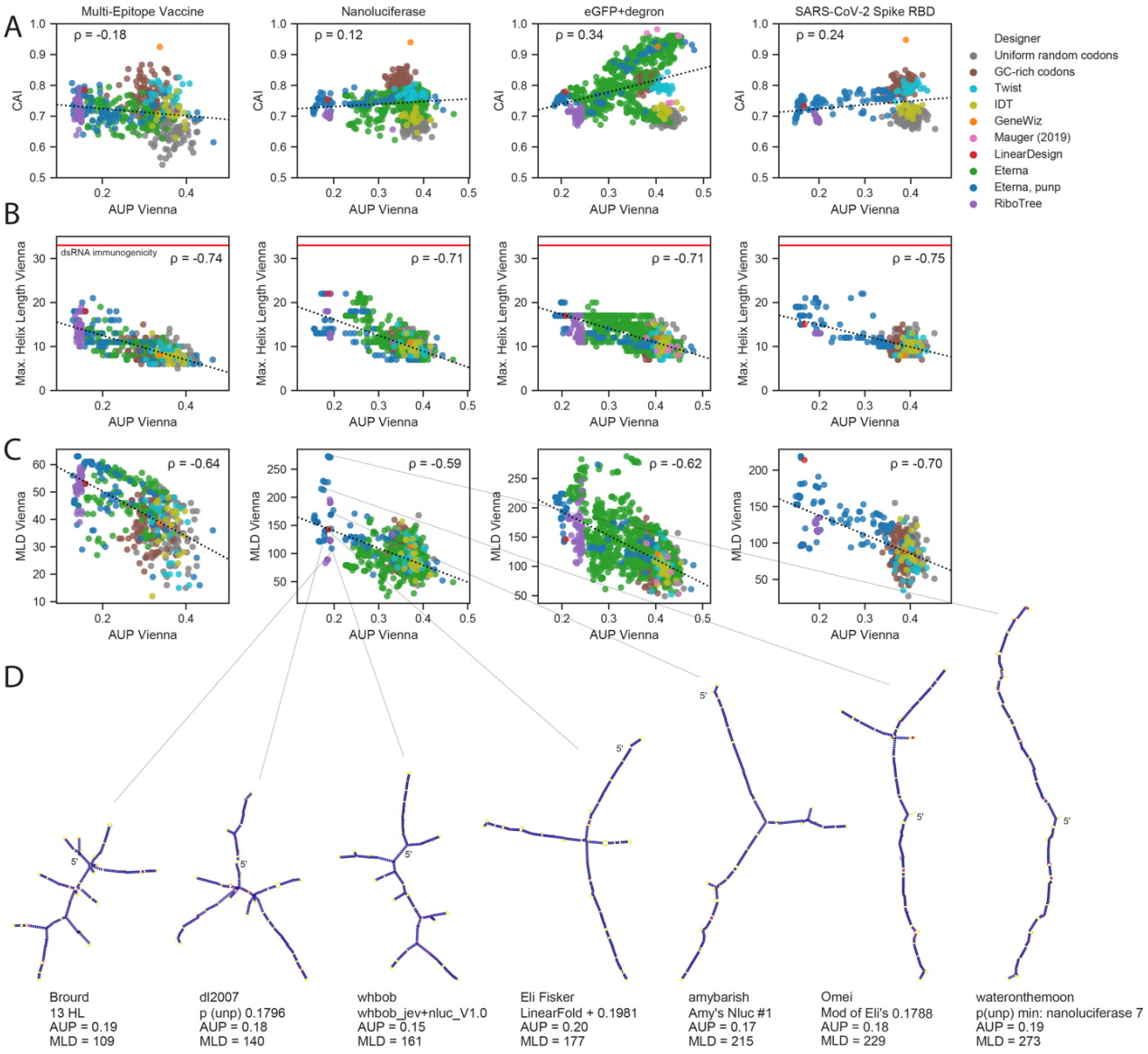

Figure 4. mRNA designs with low AUP (A) have CAI values suggestive that they are translatable, and (B) do not have helices longer than 33 nts, indicating that they are unlikely to raise an innate immune response that would shut down cellular mRNA translation. (C) Eterna designs show structural diversity as characterized by the Maximum Ladder Distance (MLD), the longest path of contiguous helices present in the MFE structure of the molecule. (D) MFE structures predicted in ViennaRNA are depicted for designs a variety of MLD values, indicating similarly stabilized stems for a range of topologies.

In addition to CAI and MLD, we calculated several other metrics characterizing structure, such as counts of different types of loops and junctions, the ratio of number of hairpins to number of 3-way junctions in the MFE structure, introduced in ref. (39) as a measure of branching, and mean distance between nucleotides in base pairs. In all cases, values ranged by over 2-fold in low-AUP solutions, underscoring the diversity of structures that can be achieved. Statistics of these metrics across the mRNA challenges and different design methods are provided in Figure S4.

Eterna participants are able to design stabilized SARS-CoV-2 full spike Protein mRNAs.

For longer mRNA design problems, including the SARS-CoV-2 full-length spike protein mRNA (3912 nts), we noted that the computational cost associated with computing thermodynamic ensembles associated with AUP became slow and hindered automated or interactive design guided by AUP. We therefore sought other observables that were more rapid to compute to guide design of RNA's stabilized against hydrolysis. We calculated correlations between many observables and AUP (Figure S5), and found that for all four challenges, the number of unpaired nucleotides in the MFE structure was the most correlated with AUP, giving near-perfect correlations (0.98, 0.99, 0.99, 0.99, respectively). We leveraged this observation to launch another puzzle on Eterna: minimizing the number of unpaired nucleotides in the MFE structure, as a proxy for AUP, for a vaccine design that includes the full SARS-CoV-2 spike protein ("full spike"). The current computational cost within the Eterna modeling interface for calculating thermodynamic ensemble statistics for the 3912-length mRNA was prohibitively slow for interactive optimization; using the number of unpaired nucleotides in the MFE structure was critical to enabling feedback to Eterna participants during their design efforts.

We found that Eterna participants were capable of finding values for AUP as low as in previous challenges, despite the fact that the full SARS-CoV-2 spike mRNA was over four times as long as previous challenges. The lowest AUP value for the full spike protein was 0.166, 2.5-fold lower than the average

AUP value from randomly sampled codon designs (0.41 +/- 0.01). Unlike other challenges, the majority of Eterna solutions for the full Spike with low AUP values shared similar sequences (Figures 5A, 5B) and structures (Figure S6). Given the diversity of structures found for other challenges such as the Nanoluciferase challenge (Figure 4C), it is likely that other low-AUP structures also exist. At this longer length, the min. AUP solution was again not the lowest ΔG(MFE) solution (Figure 5C). Promisingly, there were still no helices with lengths over 33 base pairs (Figure 5D).

Secondary structure can provide at least two-fold increases in stabilization. As a final summary of our findings, we calculated the average stabilization observed from 'standard' mRNA design methods (random codon selection, vendor optimization methods) to methods intended to enhance RNA stability through secondary structure (Eterna p(unp) challenges, RiboTree, LinearDesign). For each design method, we selected the min. AUP solution, and averaged AUP values between the 'standard' and 'improved stability' categories (Figure 5E). We found, averaged over all mRNA design challenges, approximately a two-fold change in AUP between these two categories, which was constant across mRNA length and also robust to choice of secondary structure package (Figure S7). The full spike sequence with the lowest AUP (Figure 5F), designed by Eli Fisker, had a 2.5-fold lower AUP than the average of lowest AUP solutions from conventional methods (Figure 5G).

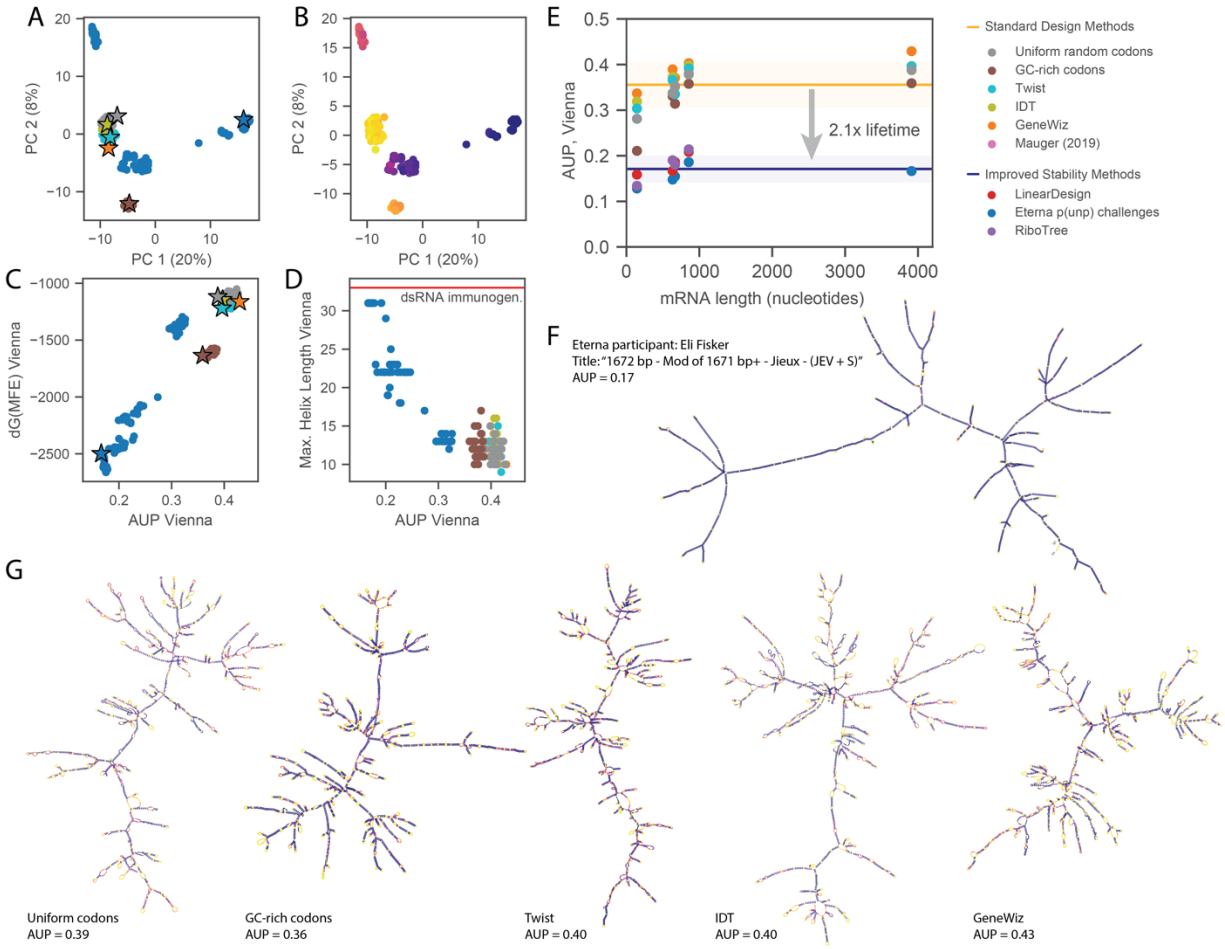

Figure 5. Eterna participants are able to design stabilized mRNAs for the SARS-CoV-2 full spike protein with the same degree of stabilization as in smaller mRNA design challenges. (A) PCA visualization of full Spike mRNA designs. (B) PCA visualization colored by AUP. (C) For full spike mRNAs, the solution with the lowest ΔG(MFE) are not the same as the sequence with the lowest AUP (both predicted with ViennaRNA). (D) Even the Eterna solutions with the lowest AUP values do not have helices longer than 33 nts (red), a threshold indicated to be the minimum helix length causing immunogenicity. (E) AUP values from different design methods are consistent across different mRNA lengths. A two-fold increase in lifetime is predicted by changing from a "Standard" design method (methods that do not stabilize structure) to a design method that increases structure. The minimal AUP sequence from Eterna (F) has a more extended conformation with fewer loops when compared to (G) minimal AUP sequences from standard design methods.

Discussion

In this work, we presented a model relating the degradation rate of an RNA molecule to the average of unpaired probabilities (AUP), a measure readily calculated in major secondary structure packages. We calculated AUP across a large collection of messenger RNA designs for small peptides, for

reporter proteins like eGFP, and for antigens under consideration for SARS-CoV-2 vaccines. The solutions with the lowest AUP values – from Eterna participants, the new RiboTree algorithm, and LinearDesign – demonstrate a 2-fold reduction in AUP from mRNAs designed through randomly selecting codons or from codon optimization algorithms from gene synthesis vendors (Figure 5E). A 2-fold reduction in AUP corresponds to a 2-fold increase in mRNA half-life, already a potentially significant improvement in the context of mRNA biotechnology. In manufacturing of mRNA, current molecules are likely being degraded substantially, with fewer than half the molecules intact at the end *in vitro* transcription; a doubling of half-life can have an exponential effect, reducing costs by more than 2-fold. During storage and delivery, pKa shifts within lipid nanoparticles and temperature excursions can bring mRNA half-lives to hydrolysis to weeks or less; a doubling of half-life may help keep the shelf-lives of mRNA in the months timescale.

Important for these practical applications, mRNAs stabilized through designed secondary structure must remain functional. The translational efficiency and immunogenicity of mRNA molecules remain difficult to predict from sequence and structure, so it is important that when designing for one property (i.e., low hydrolysis, as investigated in this work), a wide range of values for other sequence and structure features should be achievable. We were encouraged to find that low AUP designs do indeed encompass a variety of structures, as measured by maximum helix length, maximum ladder distance, number of multiloop junctions, and numerous other properties. Importantly, if future mRNA design efforts require maximizing or minimizing these sequence or structural metrics, e.g., to enhance packaging into lipid nanoparticles or to suppress innate immune responses, both Eterna crowdsourcing and the automated RiboTree framework allow for optimization of such properties simultaneously with AUP.

There are several aspects of mRNA design that remain to be addressed. An mRNA's 5' or 3' untranslated regions (UTRs) of mRNAs may interact with the coding sequence. Furthermore, there is evidence that minimizing structure at the 5' end of the CDS increases translation by minimizing the free

energy needed for the ribosome to bind (41-43). Imposing constraints of fixed UTR sequences or penalizing structure at the 5´ end of CDS can be carried out in both Eterna and RiboTree approaches, and the resulting sequences are under investigation. In addition, our optimization methods face challenges with long mRNA lengths, where the search space of potential mRNA sequences and the computational costs of predicting structural properties are larger. For the full-length Spike mRNA and longer molecules like self-amplifying mRNAs, a 'divide-and-conquer' approach may achieve lower AUP solutions, as would linearization strategies developed in the LinearFold suite of methods (29, 44). Both approaches require further exploration. Last, our analysis does not currently include modeling or design of pseudoknots or tertiary contacts due to the computational expense and inaccuracy of methods to calculate such features.

Perhaps the most important limitation of our study is the simplicity of our AUP model for degradation. The model of equations (6-9) is simple and expected to give an underestimate of how much stabilization is possible in practice. In particular, some secondary structure and sequence motifs may be less prone to hydrolysis than others (11, 16, 22). Knowledge and prioritization of those specially hydrolysis-resistant motifs in mRNA designs should lower degradation rates, perhaps surpassing the ~2-fold stabilization predicted in the present study. In preliminary work on Eterna, using a model that posits reduced hydrolysis in internal loops compared to other unpaired nucleotides leads to a 4-fold reduction in predicted hydrolysis compared to vendor-designed mRNA sequences. Critical for achieving such improvements in stability in practice will be collection of large experimental data sets mapping hydrolysis rates of many RNA's at single nucleotide resolution, and predictive models of hydrolysis rates trained on such data sets. We propose that with such empirical knowledge, mRNA lifetimes may be extended by much more than two-fold, perhaps by an order of magnitude, through computational design.

Dedication

This paper is in memory of Malcolm Watson, one of Eterna's most active participants and longtime contributors.

Acknowledgements

We thank Jonathan Romano, Andy Watkins, Sharif Ezzat, and Camilla Kao for Eterna development and assistance launching the OpenVaccine challenge and the AUP metric on the Eterna platform. We thank Ivan Zheludev for advice in designing the multi-epitope vaccine protein. We thank Eesha Sharma, Wipapat Kladwang, Kathrin Leppek, Gun Woo Byeon, Craig Kerr, Daphna Bup, other members of the Das and Barna labs (Stanford), and Mike Jewett (Northwestern University) for useful discussion regarding mRNA degradation and translation through the OpenVaccine challenge. We thank Liang Huang (Oregon State University, Baidu Research USA) for discussions of LinearDesign. RiboTree calculations were performed on the Stanford Sherlock cluster. We acknowledge funding from the National Science Foundation (GRFP to H.K.W.S. and D.S.K.), Stanford University Graduate Research Fellowship (C.A.C.), the National Institute of Health (R35 GM122579 to R.D.), and gifts to the Eterna OpenVaccine project from donors listed in Table S3.

Contributions

H.K.W.S., D.S.K., C.A.C., R.D. designed and conceptualized the research. D.S.K., R.W.O., and J.J.N. developed the Eterna interface, launched the Eterna puzzles, collected sequences, and solicited feedback from Eterna participants. C.A.C. developed the RiboTree software and performed RiboTree runs. R.A.P.S. and P.H. designed the protein sequence used in the SARS-CoV-2 Spike receptor binding domain mRNA challenge. H.K.W.S. analyzed the sequences and developed the *OpenVaccine-solves* dataset. H.K.W.S., D.S.K., and R.D. wrote the manuscript.

Methods

Data Availability. The OpenVaccine sequences and calculated features are included in the supplementary information of this manuscript. The same data, as well as scripts to reproduce analysis, are available in the "OpenVaccine-solves" database under an Open COVID license at https://eternagame.org/about/software.

Quantitative model for RNA hydrolysis. To predict the RNA degradation rates in Table 1, we used a model presented in ref. (14) for an inherent rate for phosphodiester bond cleavage as a function of pH, temperature, and ionic concentrations. The model is reproduced below:

$$k_{projected} = k_{background} \times 10^{\{0.983(pH-6)\}} \times 10^{\{-0.24(3.16-[\mathrm{K}^+])\}} \times 10^{\{0.07(T-23)\}}$$
$$\times\, 69.3\left[\mathrm{Mg}^{2+}\right]^{0.80} \times 3.57[\mathrm{K}^+]^{-0.419},$$

where $k_{background} = 1.30 \times 10^{-9}$ min^{-1}, which represents the model's selected reference point: pH 6, 23 ˚ C, [K^+] = 3.17 M. The above equation was parametrized from measurements with [Mg^{2+}] concentrations between 0.005 and 0.01 M; for conditions with 0 M Mg^{2+}, we omit the terms in the second line.

Target identification for mRNA design and optimization. Messenger RNAs encoding five target proteins were chosen for this work: 1) a candidate multi-epitope vaccine design (MEV) derived from SARS-CoV-2 Spike and Nucleocapsid proteins, 2) Nanoluciferase, 3) eGFP with a degron sequence (eGFP+deg), 4) the Receptor Binding Domain (RBD) of the SARS-CoV-2 Spike protein, and 5) the full SARS-CoV-2 Spike protein. Here we provide in detail the rationale behind how the constructs were chosen and designed.

Nanoluciferase and eGFP+degron were chosen for their ubiquitous use in biomedical research. The choice of eGFP+degron allowed for close comparison with designed mRNAs from ref. (35) , which

investigated the relationships between mRNA structure, stability and translation using the eGFP+degron, while Nanoluciferase was chosen to complement another easily assayed, commonly used model protein in mammalian systems.

For the MEV protein, we chose peptide sequences from SARS-CoV with verified T cell-positive assays that were identical in SARS-CoV-2, and one that maximized population coverage according to MHC allele mapping(45). Two of the epitopes (GYQPYRVVVL and PYRVVVLSF) map directly onto the receptor binding domain of the S (spike) protein, which we hypothesized to be important in eliciting the proper antibody/immune response. The last epitope (LSPRWYFYY), from the N protein, was chosen for its potentially high coverage of effectiveness in the global population. To test our hypothesis against a wide range of mRNA lengths, we chose to include only three peptide epitopes to introduce a shorter mRNA in our MEV design, but it should be noted that a more realistic MEV may feature many more epitopes(46, 47).

The RBD is derived from the reported structure of the spike protein in the pre-fusion conformation(48). Similarly, the protein chosen for the full spike protein is not the full sequence as found in the genome of SARS-CoV-2(1), but as reported in the pre-fusion conformation, which is hypothesized to promote an enhanced immune response in use as a vaccine. For three of the proteins (Nanoluciferase, RBD, and full spike protein), the signal sequence from the Japanese encephalitis virus (JEV) was added to the N-terminus to encode designs for a secreted vaccine(49).

Generation of vendor-optimized sequences. The protein sequences for each target (Table S2) were used to generate DNA sequences at Integrated DNA Technologies (IDT, https://www.idtdna.com/CodonOpt), Twist Biosciences (https://ecommerce.twistdna.com/app), and GENEWIZ (https://clims4.genewiz.com/Toolbox/CodonOptimization). For IDT and Twist Biosciences, multiple possible sequences were generated for a given protein sequence, while the GENEWIZ design tool returned one possible optimized DNA/RNA sequence per protein sequence.

Eterna puzzle deployment. Eterna puzzles were launched in a series of labs that can be found at the following domains: https://eternagame.org/labs/9818634, https://eternagame.org/labs/9833861, https://eternagame.org/labs/9874218, https://eternagame.org/labs/10027854, https://eternagame.org/labs/10097602, https://eternagame.org/labs/10126540. Briefly, puzzles describing the mRNA design problem were launched with a combination of the following tools: 1) the amino acid sequence and permissible codons are displayed, 2) the CAI is displayed, 3) AUP is displayed, 4) the number of base pairs formed are displayed, and 5) the MFE energy is displayed. For all puzzles, the MFE structure calculated in ViennaRNA is displayed as participants design the mRNA molecule. Each puzzle and lab features a short description of what participants should optimize for. MFE energy and MFE structure are calculated using LinearFold (44) implemented in EternaJS, and AUP is calculated using the LinearPartition (50) algorithm implemented in EternaJS.

Stochastic minimization of AUP. A Monte-Carlo Tree Search algorithm, named RiboTree, was developed to stochastically minimize AUP for mRNA sequences. RiboTree uses the Upper Confidence bounds applied to Trees (UCT) algorithm(51). The UCT loss function, as applied to the problem of sampling RNA sequences, is

$$\frac{w_i}{n_i} + c\sqrt{\frac{\ln N_i}{n_i}},$$

Where w_i is the total score considered for the node after the *i*th move, n_i is the total number of times the node was visited after the *i*th move, and c is the exploration parameter, which determines the tradeoff between depth and breadth search. For minimizing AUP, moves consist of swapping synonymous codons and are accepted with a probability

$$p(i \to j) = e^{-\beta(AUP_j - AUP_i)},$$

Where AUP_i and AUP_j are the AUP values of states i and j, respectively, and β is a temperature parameter to control the acceptance rate. The RiboTree code is available for noncommercial use upon request to the corresponding author.

LinearDesign. Solutions from LinearDesign were obtained using the LinearDesign server (http://rna.baidu.com/) and inputting the protein sequences given in Table S2. A maximum beam size of 50 was used for prediction and the standard (Human) codon table.

Metric calculations. Structure prediction and ensemble-based calculations were performed using LinearFold and LinearPartition with ViennaRNA, CONTRAfold, and EternaFold parameters. Secondary structure features were calculated from predicted MFE structures using RiboGraphViz (www.github.com/DasLab/RiboGraphViz). CAI (Codon Adaptation Index) was calculated as the geometric mean of the relative usage frequency of codons along the length of the coding region, as described in ref (52):

$$CAI = (\Pi_{i=2}{}^{L} w_i)^{L-1};\ w_i = f_i/max(f_j),$$

Where f_j represents the frequency of all codons coding for amino acid at position *i.*

Structure visualization. RNA secondary structures were visualized using draw_RNA (www.github.com/DasLab/draw_rna) and RiboGraphViz (www.github.com/DasLab/RiboGraphViz).

1. Wu, F., S. Zhao, B. Yu, Y. M. Chen, W. Wang, Z. G. Song, Y. Hu, Z. W. Tao, J. H. Tian, Y. Y. Pei, M. L. Yuan, Y. L. Zhang, F. H. Dai, Y. Liu, Q. M. Wang, J. J. Zheng, L. Xu, E. C. Holmes, and Y. Z. Zhang. 2020. A New Coronavirus Associated With Human Respiratory Disease in China. Nature 579(7798):265-269.

2. Chauhan, G., M. J. Madou, S. Kalra, V. Chopra, D. Ghosh, and S. O. Martinez-Chapa. Nanotechnology for COVID-19: Therapeutics and Vaccine Research. ACS Nano 14(7):7760-7782.

3. McKay, P. F., K. Hu, A. K. Blakney, K. Samnuan, J. C. Brown, R. Penn, J. Zhou, C. R. Bouton, P. Rogers, K. Polra, P. J. C. Lin, C. Barbosa, Y. K. Tam, W. S. Barclay, and R. J. Shattock. 2020. Self-amplifying RNA SARS-CoV-2 lipid nanoparticle vaccine candidate induces high neutralizing antibody titers in mice. Nature Communications 11(1):3523.

4. Kaczmarek, J. C., P. S. Kowalski, and D. G. Anderson. 2017. Advances in the delivery of RNA therapeutics: from concept to clinical reality. Genome Medicine 9(1):60.

5. Erasmus, J. H., and D. H. Fuller. 2020. Preparing for Pandemics: RNA Vaccines at the Forefront. Molecular Therapy 28(7):1559-1560.

6. Verbeke, R., I. Lentacker, S. C. De Smedt, and H. Dewitte. 2019. Three decades of messenger RNA vaccine development. Nano Today 28:100766.

7. Zhao, P., X. Hou, J. Yan, S. Du, Y. Xue, W. Li, G. Xiang, and Y. Dong. 2020. Long-term storage of lipid-like nanoparticles for mRNA delivery. Bioactive Materials 5(2):358-363.

8. World Health Organization. 2017. WHO preferred product characteristics for next generation influenza vaccines. World Health Organization, Geneva.

9. Zhang, N.-N., X.-F. Li, Y.-Q. Deng, H. Zhao, Y.-J. Huang, G. Yang, W.-J. Huang, P. Gao, C. Zhou, R.-R. Zhang, Y. Guo, S.-H. Sun, H. Fan, S.-L. Zu, Q. Chen, Q. He, T.-S. Cao, X.-Y. Huang, H.-Y. Qiu, J.-H. Nie, Y. Jiang, H.-Y. Yan, Q. Ye, X. Zhong, X.-L. Xue, Z.-Y. Zha, D. Zhou, X. Yang, Y.-C. Wang, B. Ying, and C.-F. Qin. 2020. A Thermostable mRNA Vaccine against COVID-19. Cell.

10. Markham, R., and J. D. Smith. 1952. The structure of ribonucleic acids. 1. Cyclic nucleotides produced by ribonuclease and by alkaline hydrolysis. Biochem J 52(4):552-557.

11. Oivanen, M., S. Kuusela, and H. Lönnberg. 1998. Kinetics and Mechanisms for the Cleavage and Isomerization of the Phosphodiester Bonds of RNA by Brønsted Acids and Bases. Chemical Reviews 98(3):961-990.

12. Cataldo, F. 2006. Ozone Degradation of Biological Macromolecules: Proteins, Hemoglobin, RNA, and DNA. Ozone: Science & Engineering 28(5):317-328.

13. Baldridge, K. C., J. Zavala, J. Surratt, K. G. Sexton, and L. M. Contreras. 2015. Cellular RNA is chemically modified by exposure to air pollution mixtures. Inhalation Toxicology 27(1):74-82.

14. Li, Y., and R. R. Breaker. 1999. Kinetics of RNA Degradation by Specific Base Catalysis of Transesterification Involving the 2'-Hydroxyl Group. J. Amer. Chem. Soc. 121(23):5364-5372.

15. Martick, M., and W. G. Scott. 2006. Tertiary Contacts Distant From the Active Site Prime a Ribozyme for Catalysis. Cell 126(2):309-320.

16. Kaukinen, U., S. Lyytikäinen, S. Mikkola, and H. Lönnberg. 2002. The Reactivity of Phosphodiester Bonds Within Linear Single-Stranded Oligoribonucleotides Is Strongly Dependent on the Base Sequence. Nucleic Acids Res. 30(2):468-74.

17. Mchedlov-Petrossyan, N. O., N. A. Vodolazkaya, A. G. Yakubovskaya, A. V. Grigorovich, V. I. Alekseeva, and L. P. Savvina. 2007. A novel probe for determination of electrical surface potential of surfactant micelles: N,N'-di-n-octadecylrhodamine. Journal of Physical Organic Chemistry 20(5):332-344.

18. Clear, K. J., K. Virga, L. Gray, and B. D. Smith. 2016. Using Membrane Composition to Fine-Tune the pKa of an Optical Liposome pH Sensor. J. Mater. Chem. C. Mater. 4(14):2925-2930.

19. Brunelle, J. L., and R. Green. 2013. Chapter Five - In Vitro Transcription from Plasmid or PCR-amplified DNA. Methods in Enzymology. J. Lorsch, editor. Academic Press, pp. 101-114.

20. Kisters, K., W. Niedner, I. Fafera, and W. Zidek. 1990. Plasma and intracellular Mg2+ concentrations in pre-eclampsia. Journal of Hypertension 8(4):303-6.

21. Geall, A. J., A. Verma, G. R. Otten, C. A. Shaw, A. Hekele, K. Banerjee, Y. Cu, C. W. Beard, L. A. Brito, T. Krucker, D. T. O'Hagan, M. Singh, P. W. Mason, N. M. Valiante, P. R. Dormitzer, S. W. Barnett, R. Rappuoli, J. B. Ulmer, and C. W. Mandl. 2012. Nonviral delivery of self-amplifying RNA vaccines. Proc. Natl. Acad. Sci. 109(36):14604-9.

22. Mikkola, S., U. Kaukinen, and H. Lönnberg. 2001. The Effect of Secondary Structure on Cleavage of the Phosphodiester Bonds of RNA. Cell Biochem. Biophys. 34(1):95-119.

23. Regulski, E. E., and R. R. Breaker. 2008. In-line Probing Analysis of Riboswitches. Methods Mol. Biol. 419:53-67.

24. Lorenz, R., S. H. Bernhart, C. Honer Zu Siederdissen, H. Tafer, C. Flamm, P. F. Stadler, and I. L. Hofacker. 2011. ViennaRNA Package 2.0. Algorithms Mol. Biol. 6:26.

25. Zadeh, J. N., C. D. Steenberg, J. S. Bois, B. R. Wolfe, M. B. Pierce, A. R. Khan, R. M. Dirks, and N. A. Pierce. 2011. NUPACK: Analysis and design of nucleic acid systems. J Comput Chem 32(1):170-173.

26. Reuter, J. S., and D. H. Mathews. 2010. RNAstructure: software for RNA secondary structure prediction and analysis. BMC Bioinformatics 11:129.

27. Do, C. B., D. A. Woods, and S. Batzoglou. 2006. CONTRAfold: RNA secondary structure prediction without physics-based models. Bioinformatics 22(14):e90-98.

28. Terai, G., S. Kamegai, and K. Asai. 2016. CDSfold: An Algorithm for Designing a Protein-Coding Sequence With the Most Stable Secondary Structure. Bioinformatics 32(6):828-34.

29. Zhang, H., L. Zhang, Z. Li, K. Liu, B. Liu, D. H. Mathews, and L. Huang. 2020. LinearDesign: Efficient Algorithms for Optimized mRNA Sequence Design. Arxiv.

30. Cohen, B., and S. Skiena. 2003. Natural Selection and Algorithmic Design of mRNA. Journal of Computational Biology 10(3-4):419:32.

31. Zhao, X., G. Li, and S. Liang. 2013. Several Affinity Tags Commonly Used in Chromatographic Purification. J. Anal. Methods Chem. 2013:581093.

32. Presnyak, V., N. Alhusaini, Y. H. Chen, S. Martin, N. Morris, N. Kline, S. Olson, D. Weinberg, K. E. Baker, B. R. Graveley, and J. Coller. 2015. Codon optimality is a major determinant of mRNA stability. Cell 160(6):1111-1124.

33. Hanson, G., and J. Coller. 2018. Codon optimality, bias and usage in translation and mRNA decay. Nat. Rev. Mol. Cell. Biol. 19(1):20-30.

34. Wayment-Steele, H. K., W. Kladwang, E. Participants, and R. Das. 2020. RNA secondary structure packages ranked and improved by high-throughput experiments. bioRxiv.

35. Mauger, D. M., B. J. Cabral, V. Presnyak, S. V. Su, D. W. Reid, B. Goodman, K. Link, N. Khatwani, J. Reynders, M. J. Moore, and I. J. McFadyen. 2019. mRNA structure regulates protein expression through changes in functional half-life. Proc Natl Acad Sci U S A 116(48):24075-24083.

36. Lee, J., W. Kladwang, M. Lee, D. Cantu, M. Azizyan, H. Kim, A. Limpaecher, S. Yoon, A. Treuille, and R. Das. 2014. RNA design rules from a massive open laboratory. Proc Natl Acad Sci U S A 111(6):2122-2127.

37. Hur, S. 2019. Double-Stranded RNA Sensors and Modulators in Innate Immunity. Annu Rev Immunol 37:349-375.

38. Yoffe, A. M., P. Prinsen, A. Gopal, C. M. Knobler, W. M. Gelbart, and A. Ben-Shaul. 2008. Predicting the sizes of large RNA molecules. Proc Natl Acad Sci U S A 105(42):16153-16158.

39. Gopal, A., D. E. Egecioglu, A. M. Yoffe, A. Ben-Shaul, A. L. N. Rao, C. M. Knobler, and W. M. Gelbart. 2014. Viral RNAs Are Unusually Compact. PLoS One 9(9):e105875.

40. Karikó, K., H. Ni, J. Capodici, M. Lamphier, and D. Weissman. 2004. mRNA Is an Endogenous Ligand for Toll-like Receptor 3. J. Biol. Chem. 279(13):12542-12550.

41. Ding, Y., Y. Tang, C. K. Kwok, Y. Zhang, P. C. Bevilacqua, and S. M. Assmann. 2014. In vivo genome-wide profiling of RNA secondary structure reveals novel regulatory features. Nature 505(7485):696-700.

42. Wan, Y., K. Qu, Q. C. Zhang, R. A. Flynn, O. Manor, Z. Ouyang, J. Zhang, R. C. Spitale, M. P. Snyder, E. Segal, and H. Y. Chang. 2014. Landscape and variation of RNA secondary structure across the human transcriptome. Nature 505(7485):706-9.

43. Pop, C., S. Rouskin, N. T. Ingolia, L. Han, E. M. Phizicky, J. S. Weissman, and D. Koller. 2014. Causal signals between codon bias, mRNA structure, and the efficiency of translation and elongation. Molecular Systems Biology 10(12):770.

44. Huang, L., H. Zhang, D. Deng, K. Zhao, K. Liu, D. A. Hendrix, and D. H. Mathews. 2019. LinearFold: linear-time approximate RNA folding by 5'-to-3' dynamic programming and beam search. Bioinformatics 35(14):i295-i304.

45. Ahmed, S. F., A. A. Quadeer, and M. R. McKay. 2020. Preliminary Identification of Potential Vaccine Targets for the COVID-19 Coronavirus (SARS-CoV-2) Based on SARS-CoV Immunological Studies. Viruses 12(3):254.

46. Qamar, M. T. u., A. Rehman, U. A. Ashfaq, M. Q. Awan, I. Fatima, F. Shahid, and L.-L. Chen. 2020. Designing of a next generation multiepitope based vaccine (MEV) against SARS-COV-2: Immunoinformatics and in silico approaches. bioRxiv.

47. Prachar, M., S. Justesen, D. B. Steen-Jensen, S. Thorgrimsen, E. Jurgons, O. Winther, and F. O. Bagger. 2020. COVID-19 Vaccine Candidates: Prediction and Validation of 174 SARS-CoV-2 Epitopes. bioRxiv.

48. Wrapp, D., N. Wang, K. S. Corbett, J. A. Goldsmith, C.-L. Hsieh, O. Abiona, B. S. Graham, and J. S. McLellan. 2020. Cryo-EM structure of the 2019-nCoV spike in the prefusion conformation. Science 367(6483):1260-1263.

49. Liu, H., R. Wu, L. Yuan, G. Tian, X. Huang, Y. Wen, X. Ma, Y. Huang, Q. Yan, Q. Zhao, S. Cao, and X. Wen. 2017. Introducing a Cleavable Signal Peptide Enhances the Packaging Efficiency of Lentiviral Vectors Pseudotyped With Japanese Encephalitis Virus Envelope Proteins. Virus research 229:9-16.

50. Zhang, H., L. Zhang, D. H. Mathews, and L. Huang. 2020. LinearPartition: linear-time approximation of RNA folding partition function and base-pairing probabilities. Bioinformatics 36(Supplement_1):i258-i267.

51. Kocsis, L., and C. Szepesvári. 2006. Bandit Based Monte-Carlo Planning. Springer Berlin Heidelberg, Berlin, Heidelberg. 282-293.

52. Sharp, P. M., and W. H. Li. 1987. The codon Adaptation Index--a measure of directional synonymous codon usage bias, and its potential applications. Nucleic Acids Res 15(3):1281-1295.